nature neuroscience

Slow integration leads to persistent action potential firing in distal axons of coupled interneurons

Mark E J Sheffield[1], Tyler K Best[1], Brett D Mensh[2], William L Kath[1,3] & Nelson Spruston[1]

The conventional view of neurons is that synaptic inputs are integrated on a timescale of milliseconds to seconds in the dendrites, with action potential initiation occurring in the axon initial segment. We found a much slower form of integration that leads to action potential initiation in the distal axon, well beyond the initial segment. In a subset of rodent hippocampal and neocortical interneurons, hundreds of spikes, evoked over minutes, resulted in persistent firing that lasted for a similar duration. Although axonal action potential firing was required to trigger persistent firing, somatic depolarization was not. In paired recordings, persistent firing was not restricted to the stimulated neuron; it could also be produced in the unstimulated cell. Thus, these interneurons can slowly integrate spiking, share the output across a coupled network of axons and respond with persistent firing even in the absence of input to the soma or dendrites.

The brain processes information using billions of interconnected neurons. Efforts to understand how such information processing works in neural circuits are usually based on the notion that information flows into the dendrites and out along the axon. This is known as the law of dynamic polarization, part of Ramón y Cajal's neuron doctrine[1]. There are exceptions to this, including neurons that lack dendrites or an axon[2–4], as well as action potentials propagating from the axon into dendrite[5]. In invertebrates, action potentials can originate in multiple sites, including axon terminals[6–8], but in the mammalian CNS, the evidence for spike initiation in axon terminals is mostly limited to pathological conditions such as epilepsy[9]. We found that action potentials could be initiated in the distal axon under normal conditions and in response to natural firing patterns. We also found that axonal arborizations can communicate with each other without the need for intervening synapses onto dendrites or somata and that this form of firing results from integration that occurs on a timescale of tens of seconds to minutes and can result in firing for a similarly long period of time.

RESULTS

We performed patch-clamp recordings from interneurons that expressed enhanced green fluorescent protein (EGFP) near the border of the stratum radiatum and stratum lacunosum-moleculare (SLM) of hippocampal area CA1 in acute slices prepared from serotonin 5b receptor (*Htr5b*) BAC transgenic mice (GENSAT[10], see Online Methods). *Post hoc* staining of biocytin-filled interneurons revealed that these EGFP-positive interneurons had dendrites that were contained in the CA1 region. The axonal arborization was larger than the dendritic tree and occasionally extended into the neighboring CA3 region or subiculum, or crossed the hippocampal fissure to enter the dentate gyrus (**Fig. 1a**). On the basis of their location and dendritic and axonal arborizations, these are most likely perforant path–associated inhibitory interneurons[11] (**Supplementary Table 1**).

Persistent firing in hippocampal interneurons

In ~80% of the EGFP-positive interneurons (n = 214 of 274), repeated somatic current injections eventually triggered persistent firing that outlasted the current injection by seconds or minutes (**Fig. 1b,c** and **Supplementary Fig. 1**). Once initiated, the persistent firing frequency increased to a maximum firing rate of 52.1 ± 1.9 Hz occurring at 3.5 ± 0.2 s after the end of the final stimulus (n = 187; **Fig. 1d** and **Supplementary Fig. 2**). In most neurons, persistent firing lasted for tens of seconds; the median duration was 58 s (n = 180) and seven outlier cells had durations of 4–13 min (**Fig. 1e**).

Persistent firing was not an artifact of BAC transgenic EGFP expression, as it was observed in 24% (n = 13 of 54) of EGFP-negative hippocampal interneurons in the Htr5b mice, 8% (n = 1 of 13) of EGFP-positive hippocampal interneurons in Drd2 BAC transgenic mice and 23% (n = 6 of 26) of hippocampal interneurons in wild-type C57BL/6 mice (**Supplementary Fig. 3**). We also observed persistent firing in 17% of CA1 interneurons in rat hippocampal slices (n = 3 of 18), indicating that it occurs across species (**Supplementary Fig. 3**). These findings suggest that the persistent-firing interneurons are selectively labeled in *Htr5b* BAC transgenic mice. Given that persistent firing can be induced in interneurons of wild-type mice and rats, it is surprising that it has not been reported previously. One possibility is that it has been observed, but not reported, because it does not occur in all cells, thus making it hard to study systematically. Another possibility is that it has not been observed because slice physiologists typically do not stimulate cells with hundreds of action potentials (for example, **Supplementary Fig. 1c**). Finally, persistent firing may have been missed because it is temperature sensitive; it was only observed near physiological temperatures and never at 20–22 °C (Online Methods).

Persistent firing could also be induced in EGFP-positive interneurons of somatosensory cortex (**Fig. 1f**), although with a lower probability than in the hippocampus (n = 7 of 19 cells, 37% versus 78% in hippocampus,

[1]Department of Neurobiology & Physiology, Northwestern University, Evanston, Illinois, USA. [2]Department of Physical Medicine and Rehabilitation, Harvard Medical School, Boston, Massachusetts, USA. [3]Department of Engineering Sciences and Applied Math, Northwestern University, Evanston, Illinois, USA. Correspondence should be addressed to N.S. (spruston@northwestern.edu).

Received 27 August; accepted 1 December; published online 8 December 2010; doi:10.1038/nn.2728

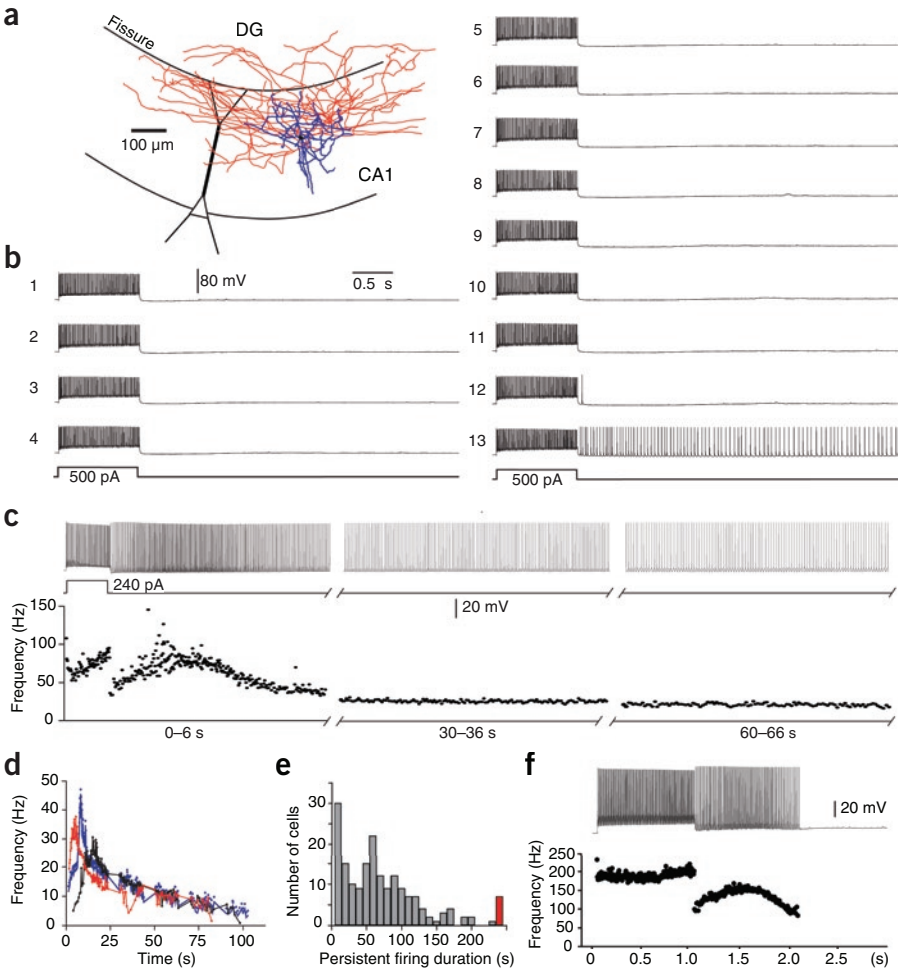

Figure 1 Persistent firing in Htr5b interneurons. (**a**) A biocytin-filled Htr5b-EGFP–positive interneuron near the stratum radiatum–SLM border of hippocampal area CA1 (dendrites, blue; axon, red). A schematic representation of a CA1 pyramidal cell is also shown (DG, dentate gyrus). (**b**) Whole-cell current-clamp recording of persistent firing. To evoke persistent firing, we delivered a 1-s current step of 500 pA during each 10-s sweep (left, sweeps 1–4; right, sweeps 5–13). In this example, the total number of evoked action potentials before persistent firing was 1,151. (**c**) Persistent firing was also induced with 1-s current steps starting at 40 pA and incrementing the amplitude by 20 pA with each subsequent step (shown here is the response to the 11th step, 240 pA, which induced persistent firing after a total of 296 action potentials). In this example, persistent firing lasted over 1 min. The instantaneous firing frequency of each action potential is plotted below the recording. (**d**) Three representative cells showing the frequency of persistent firing over time after its onset. (**e**) Persistent firing duration measured from its onset to the last spike ($n = 274$). The red bar shows the cells where persistent firing outlasted the 4-min recording period ($n = 5$). (**f**) Persistent firing in a layer 2/3 neocortical interneuron (somatosensory cortex) induced with the same protocol used in **c**; only the final trace is shown. All data are from Htr5b-EGFP–positive hippocampal interneurons near the stratum radiatum–SLM border.

$P < 0.0001$). In addition, more spikes were required to induce persistent firing in neocortical interneurons (neocortex, 1,821 ± 381; hippocampus, 792 ± 32), the resulting maximum persistent-firing frequency was higher (neocortex, 123 ± 13 Hz; hippocampus, 53 ± 2 Hz), was reached more quickly (neocortex, 1.2 ± 0.5 s from end of triggering stimulus; hippocampus, 3.5 ± 0.2 s) and the duration of persistent firing was shorter (neocortex, median = 2.6 s; hippocampus, median = 58 s; **Supplementary Fig. 4a–e**). These observations indicate that all aspects of persistent firing are more rapid in neocortex than in hippocampus.

In addition to step current injections, synaptic stimulation or sine wave current injections (mimicking theta oscillations) could also induce persistent firing (**Supplementary Fig. 5**). In EGFP-positive interneurons of *Htr5b* BAC transgenic mice, antidromic stimulation during cell-attached recording also elicited persistent firing, indicating that persistent firing is not an artifact of cytoplasmic washout during whole-cell recording. We induced persistent firing using antidromic stimulation in the presence of blockers for glutamate and GABA receptors (Online Methods), indicating that activation of AMPA, NMDA, $GABA_A$ and $GABA_B$ receptors was not required for persistent firing (**Supplementary Fig. 5**). With all of these methods, multiple stimuli were required to induce persistent firing. After persistent firing ceased, the neuron could be stimulated again to produce another epoch of persistent firing (Online Methods), indicating that persistent firing was not caused by a decline in cell heath or recording quality.

Persistent firing in response to natural spike trains

To determine whether persistent firing could occur in response to physiologically relevant spiking patterns, we stimulated these cells using spike trains that were acquired from *in vivo* recordings of hippocampal interneurons (see Online Methods for details). Both a low-frequency pattern from a perforant path–associated interneuron in an anesthetized rat[12] (5.8-Hz mean; **Fig. 2a**) and a higher frequency pattern from a hippocampal interneuron in an awake rat (S. Layton and M. Wilson, unpublished data, 33-Hz mean; **Fig. 2b**) induced persistent firing efficiently (**Fig. 2c**). The high-frequency pattern was the most effective at evoking persistent firing (step/pause, 19/22; low frequency, 16/22; high frequency, 14/14 cells). The reliability of natural spike trains to elicit persistent firing suggests that persistent firing is not an artifact of excessive spiking.

The number of spikes required to induce persistent firing was significantly less when using the low-frequency and high-frequency *in vivo* patterns compared with the step/pause protocol in the same cells ($P < 0.01$), whereas the number of spikes required using the high- and low-frequency patterns were not different (**Fig. 2d**,**e**). The latency to persistent firing (defined as the time from the first evoked spike to the first persistent-firing spike) was significantly longer for the step/pause protocol than for either the low-frequency or high-frequency *in vivo* patterns ($P < 0.01$; **Fig. 2f**,**g**). The latency was also significantly less for the high-frequency than for the low-frequency *in vivo* pattern ($P < 0.001$).

The effectiveness of the *in vivo* firing patterns is likely a result of the absence of the long (9 s) pauses that are present in the current-step protocol. The high-frequency *in vivo* firing protocol required only ~20% fewer spikes than the low-frequency *in vivo* protocol, but induction occurred sooner (that is, those spikes occurred in a much shorter period of time), suggesting that the total number of evoked spikes is more important than the frequency of the evoked spikes for triggering persistent firing.

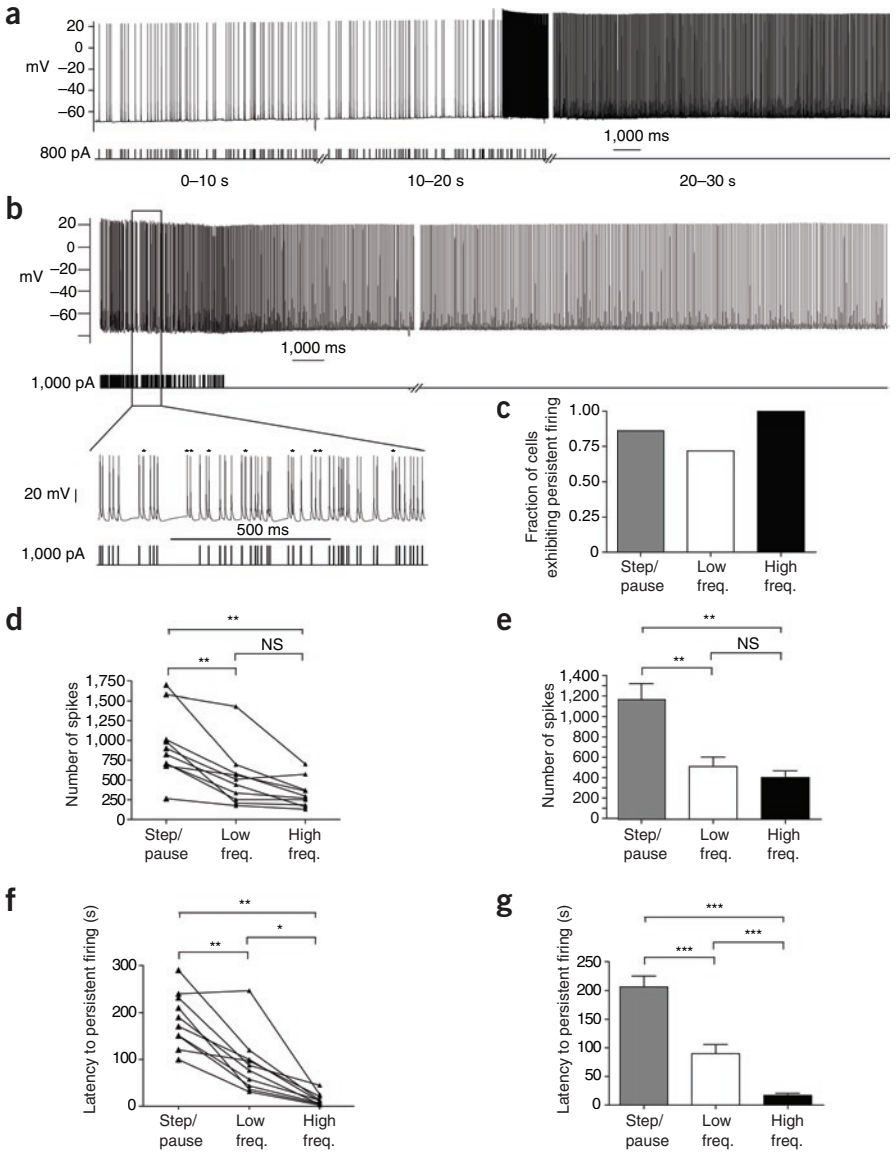

Figure 2 *In vivo* firing patterns induce persistent firing. (**a**,**b**) Persistent firing evoked by low (**a**) and high (**b**) frequency *in vivo* firing patterns. Bottom left, expanded segment of the high frequency *in vivo* firing pattern and corresponding evoked spikes. Asterisks indicate spikes that have no corresponding stimulus and thus indicate the onset of persistent firing during the stimulus period. (**c**) Comparison of the fraction of cells that generated persistent firing with various stimulation protocols. Step/pause ($n = 19$) is the protocol described in **Figure 1c** and **Supplementary Figure 1a**; low ($n = 16$) and high ($n = 14$) frequency refer to the *in vivo* firing patterns shown in **a** and **b**, respectively. (**d**,**e**) The total number of evoked spikes needed to generate persistent firing showed no difference between the low- and high-frequency protocols, but both were less than the step/pause protocol. (**d**) Within-cell comparisons ($n = 10$). (**e**) Grouped data comparisons (step/pause, $n = 19$; low frequency, $n = 16$; high frequency, $n = 14$). (**f**,**g**) The latency to persistent firing was shortest for the high-frequency protocol. (**f**) Within cell comparisons ($n = 10$). (**g**) Grouped data comparisons (step/pause, $n = 19$; low frequency, $n = 16$; high frequency, $n = 14$). Latency to persistent firing was greatest using the step/pause protocol. All summary data consist of mean ± s.e.m. $^{***}P < 0.001$, $^{**}P < 0.01$, $^{*}P < 0.05$. All data are from Htr5b-EGFP–positive hippocampal interneurons near the stratum radiatum–SLM border.

Persistent firing follows slow integration of spikes

Regardless of the stimulation method used, hundreds of evoked spikes were required to trigger persistent firing (**Fig. 2d,e**) and these spikes were evoked over durations ranging from tens of seconds to minutes (**Fig. 2f,g**). These findings indicate that spikes can be integrated over long periods of time, consistent with a leaky integrator having a long decay time constant.

To quantify the nature of the integrator, we fit the data from the *in vivo* and step/pause firing patterns used for induction. Different datasets produced different optimal fits, but in all cases there was a threshold of 270–380 integrated spikes and a decay time constant of 50–150 s. This simple model implies the existence of a mechanism that encodes the firing history of the neuron with a time constant of more than a minute.

Persistent firing is initiated in the distal axon

In contrast with spiking evoked with somatic current injection, during persistent firing there was no envelope of depolarization in the somatic patch-clamp recording; spikes arose abruptly from a membrane potential near rest (apparent action potential threshold −67.7 ± 0.3 mV; **Fig. 3a,b**). The mean action potential threshold for the initial 9 s of persistent firing was −68.8 ± 0.5 mV compared with a mean holding potential of −66.8 mV. The apparent spike threshold was more depolarized after longer periods of persistent firing, but always remained about 20 mV below the threshold for current-evoked action potentials (**Supplementary Table 1**). This feature of persistent spikes was similar to that of spikes evoked by antidromic stimulation of the axon (**Fig. 3c,d**), suggesting that persistent firing originates in the axon. Phase plots revealed that antidromic and spontaneous spikes had two components: an initial component represented spiking in the axon and a second component that overlapped with the current-evoked spikes, indicative of a somato-dendritic spike that follows the initial, axonally initiated spike (**Fig. 3d**).

In some recordings ($n = 11$), partial spikes (spikelets) were observed during persistent firing (**Fig. 3e** and **Supplementary Fig. 4f**). These spikelets overlapped with the first portion of the full-amplitude spikes, with the peak of the spikelets corresponding to an inflection on the rising phase seen in the full-amplitude spikes. This is seen more clearly in the phase plots of a spikelet, full-amplitude spike during persistent firing and an evoked somatic spike (**Fig. 3f**). Note that the phase plot of the evoked action potential has one component with the same peak $dV\,dt^{-1}$ as the spikelet and a second component with a peak matching the spike during persistent firing. These observations suggest that the first component of each action potential during persistent firing is an axonal spike, which sometimes fails to evoke a somato-dendritic spike. In some cells ($n = 3$), spikelets were observed during somatic hyperpolarization (**Fig. 3g**). An expanded view of the initial part of the phase plot (**Fig. 3h**) again revealed an inflection point where the persistent firing

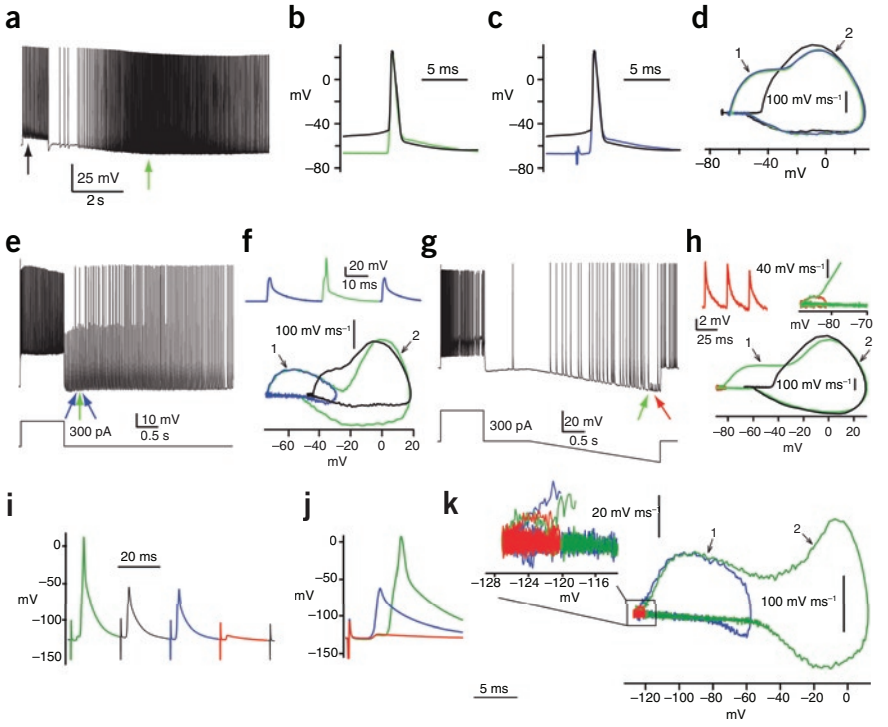

Figure 3 Full-sized action potentials and large and small spikelets during persistent firing match antidromic full and partial spikes. (**a**) Persistent firing with somatically evoked (for example, black arrow) and persistent firing (for example, green arrow) action potentials indicated. (**b**) Somatically evoked (black) and persistent firing (green) action potentials, peak aligned. (**c**) Antidromic (blue) and somatically evoked action potentials (black) from the same cell in **a**, peak aligned. (**d**) Phase plot ($dV\,dt^{-1}$ versus V) of action potentials from **b** and **c** (stimulus artifact eliminated). The numbers 1 and 2 on all phase plots indicate presumed axonal and somatic firing, respectively. (**e**) Spontaneous large spikelets during persistent firing ($n = 6$). (**f**) Expanded view (top) of large spikelets (blue) and a full-sized spike (green) taken from **e** (blue and green arrows). Phase plots (bottom) of a large spikelet (blue), evoked (black) and persistent-firing action potentials (green) are shown. (**g**) Hyperpolarization in this cell revealed small spikelets. (**h**) Top left, expanded view of the spikelets in **g**. Phase plots (bottom) of a small spikelet (red), evoked (black) and persistent-firing (green) action potentials are shown. Top right, expanded view of the initial part of the phase plot. (**i**) Full action potential (green) and large (black and blue) and small spikelets (red) evoked by antidromic stimulation during somatic hyperpolarization to –125 mV in the presence of glutamate and GABA receptor blockers. (**j**) Colored spikes from **i** overlaid and aligned by the stimulus artifacts. (**k**) Phase plot from the spikes in **j** (right) with expanded view (left). All data are from Htr5b-EGFP–positive hippocampal interneurons near the stratum radiatum–SLM border.

action potential follows the phase plot of the spikelet. These spikelets were smaller than those observed without hyperpolarization, suggesting that they are caused by propagation failures at a more distal axonal location (**Fig. 3h**) than the failure point of the larger spikelets (**Fig. 3e,f**). The spikelets described here (that is, presumed to be caused by failure of axonal action potential propagation to the soma) were easily distinguishable from other spikelets that appeared to be from spikes in cells connected by gap junctions (**Supplementary Fig. 6**).

Persistent firing continued during somatic hyperpolarization and the apparent spike threshold decreased as the soma was hyperpolarized (**Fig. 3g**), suggesting that the spikes are generated in an electrotonically remote location. In some cells, persistent firing appeared to cease during hyperpolarization of the soma ($n = 11$ of 21), but resumed without delay on removal of the hyperpolarizing current (**Supplementary Fig. 7**). In these instances, we are unable to distinguish between true cessation of firing and continued axonal spiking with failure of these spikes to invade the soma.

Spikelets were also observed in response to antidromic stimulation of the axon while hyperpolarizing the soma with current injection. In some cases, antidromic spikelets with two different amplitudes were observed in the same cell ($n = 9$; **Fig. 3i–k**). Phase plots of these spikelets revealed that the large spikelet followed the initial component of the full action potential (**Fig. 3k**) in much the same way that the large spikelet followed the full action potential during persistent firing (**Fig. 3f**). The phase plot also showed that the small antidromic spikelet overlapped the initial component of the large spikelet and full action potential, suggesting that these small events give rise to the larger ones, as observed during persistent firing.

Using a simple computational model of a branching axon attached to a soma, we simulated both small- and large-amplitude spikelets, as well as full-amplitude spikes, by depolarizing a branch of the axon during somatic hyperpolarization. Large-amplitude spikelets corresponded to failure of the action potential to invade the soma, whereas small-amplitude spikelets corresponded to failures at the axon branches, 40 μm from the soma (**Fig. 4a–c** and **Supplementary Movie 1**). Similar results were obtained with a full morphological model of a branching axonal arborization (**Fig. 4d–f** and **Supplementary Movie 2**).

Persistent firing does not require somatic depolarization

To further test the hypothesis that persistent firing is generated in the axon, we induced it by delivering antidromic stimuli repeatedly. Antidromic stimulation was applied in the dentate gyrus, a region frequently containing branches of the axon, but never the dendrites of the CA1 interneurons that we targeted. These experiments were also performed in the presence of glutamate and GABA receptor blockers to prevent synaptic activation of dendrites (Online Methods). When antidromic stimulation was performed repeatedly (increasing the frequency of stimuli in subsequent sweeps), persistent firing could be induced, even while holding the somatic membrane potential at a hyperpolarized level that reduced or eliminated somatic spiking during the antidromic stimulation ($n = 5$; **Fig. 5a,b**). Under these conditions, small-amplitude spikelets were recorded at the soma in response to most antidromic stimuli and represented propagation failures of antidromic-evoked spikes that looked similar to spikelets during persistent firing (**Fig. 3e–h**). Persistent action potential firing was nevertheless observed after both the antidromic stimulus and the hyperpolarizing current injection ceased (**Fig. 5b**). These results support the hypothesis that persistent firing is generated in the distal axon and that it can be generated even in the absence of depolarization of the dendrites, soma or proximal axon.

To test for cell coupling during persistent firing, we recorded from 19 pairs of EGFP-positive hippocampal interneurons (**Fig. 5c**). None of these pairs exhibited obvious chemical synaptic coupling; electrical

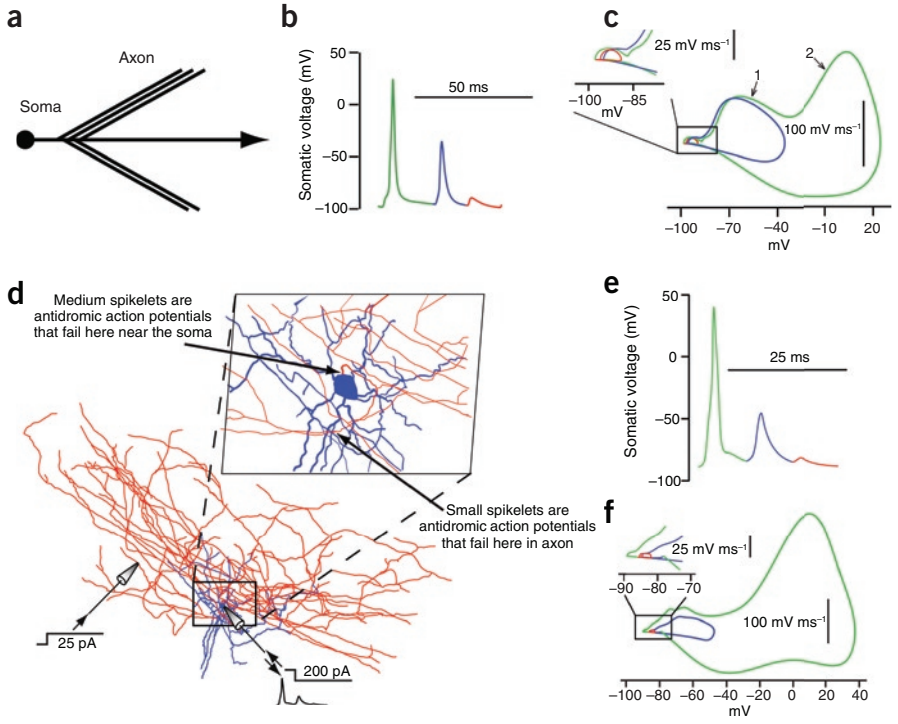

Figure 4 Simulation of small and large spikelets indicates failure of antidromic action potentials at different locations along the axon. (**a**) Morphology of a stylized interneuron model, with a spherical soma connected to a primary axon with five side branches. (**b**) Somatic voltage trace in the stylized model as a result of distal axonal depolarization (960 µm from soma) during simultaneous somatic hyperpolarization. The resulting antidromic action potentials occurred in a repeating pattern consisting of a full action potential (green), an antidromic action potential that fails at the soma (blue) and three small spikelets (red, only one shown) corresponding to action potential failure at an axonal branch point. (**c**) Phase plot of traces from **b**. Inset shows expanded view. (**d**) Morphology of a fully reconstructed interneuron with its cell body near the stratum radiatum–SLM border showing soma and dendrites (blue), axon (red) and locations of the axonal and somatic stimulating and recording electrodes. Inset, expanded view showing the two different points at which antidromic axonal action potentials fail. (**e**) Voltage trace in the full morphological model as a result of distal axonal depolarization (325 µm from the soma) during simultaneous somatic hyperpolarization. Antidromic action potentials were generated and produced a repeating somatic voltage pattern consisting of a full action potential (green), an antidromic action potential that fails at the soma (blue) and an antidromic action potential that fails at an axonal branch point (brown). (**f**) Phase plot of traces from **e**. Inset shows expanded view.

coupling was observed in 6 of 19 pairs. To induce persistent firing, only one of the two cells was stimulated with step current injections. In 16 of 19 cases, persistent firing was only observed in the stimulated neuron. In the other three pairs, persistent firing was induced in the unstimulated neuron (**Fig. 5d**); none of these three pairs exhibited direct electrical coupling. In two of these three pairs, persistent firing developed in the unstimulated neuron, but not in the stimulated neuron (**Fig. 5d**). In the third pair, persistent firing began in the stimulated neuron and then stopped, followed by persistent firing in the unstimulated neuron. In all three pairs, similar behavior recurred when the same stimulus was delivered again, indicating that the persistent firing was triggered by the stimulus. In all of our single-cell recordings ($n = 274$), we never saw persistent firing develop spontaneously. Thus, the observation of persistent firing in 3 of 19 unstimulated cells is a highly statistically significant indication ($P < 0.001$) that persistent firing can be induced by stimulating another cell (Online Methods). These results are consistent with a form of intercellular signaling that promotes the induction of persistent firing in a network of sparsely connected interneurons.

Clues regarding the mechanisms of persistent firing

Elucidating the mechanisms responsible for persistent firing will be complex, as several questions must be addressed. What mechanisms

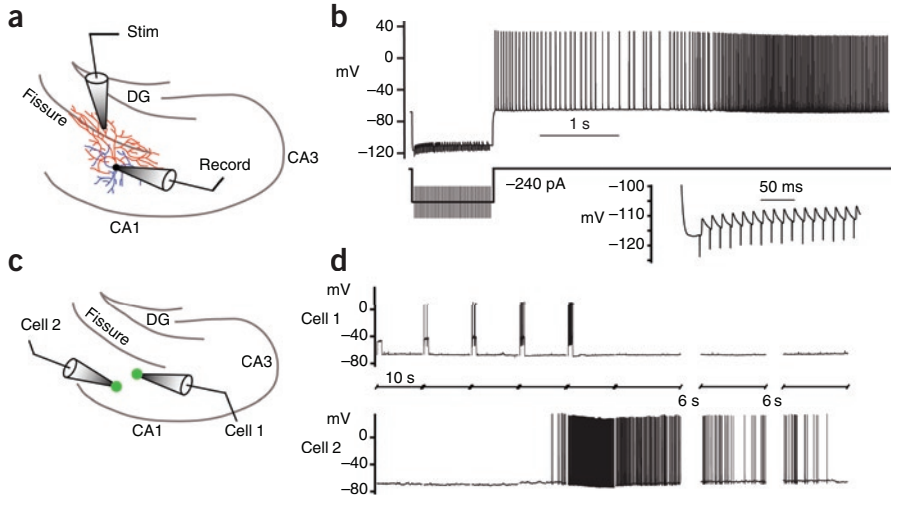

Figure 5 Persistent firing induced by antidromic stimulation and intercellular signaling. (**a**) Diagram depicting recording setup (axon red, dendrites blue). For antidromic stimulation, the stimulating electrode was placed in the molecular layer of the dentate gyrus to activate only axonal projections. (**b**) Antidromic stimulation of the axon during simultaneous somatic hyperpolarization also evoked persistent firing (in the presence of glutamate and GABA receptor blockers; see Online Methods). The inset shows failed spikes during antidromic stimulation. The number of stimuli was increased by two during each successive stimulus until persistent firing occurred. Persistent firing was reliably induced in this manner ($n = 5$). (**c**) Illustration of paired recording setup. Step current injections were delivered to cell 1 only. Interneurons near the stratum radiatum–SLM border and in the stratum radiatum were targeted. (**d**) Persistent firing was induced in the unstimulated cell and occurred before persistent firing was induced in the stimulated cell. No electrical coupling was observed between the pairs. In total, 19 Htr5b-EGFP–positive pairs were studied, with three showing this type of intercellular induction of persistent firing.

allow hundreds of action potentials to be integrated on a timescale of tens of seconds to minutes? How is this integrated signal detected by more than just the stimulated neuron? What conductances are modulated to depolarize the axon and generate persistent firing? We made two important observations that will facilitate future studies of these mechanistic questions.

First, we found that lowering extracellular Ca^{2+} did not prevent persistent firing or affect the number of spikes needed to induce it ($n = 20$ for 0, 0.5 and 1 mM Ca^{2+}; **Fig. 6a–c**). This result suggests that neither Ca^{2+}-dependent exocytosis nor a Ca^{2+} conductance is likely to be required for persistent firing. However, lower Ca^{2+} concentrations did lead to longer-lasting persistent firing, suggesting that Ca^{2+} entry may participate in the termination of persistent firing.

Second, we found that two gap junction–inhibiting drugs (mefloquine and carbenoxelone) prevented the induction of persistent firing (**Fig. 7a,b**). In these experiments, persistent firing was not induced in the presence of either drug, even when the number of evoked action potentials far exceeded that required to induce persistent firing in the same cells before drug application ($n = 10$; **Fig. 7c,d**). Although the action of these drugs was not reversed, in the absence of gap junction blockers we were able to induce persistent firing repeatedly in every cell where we attempted to do so, including 101 cells in which persistent firing was induced five times or more. These results indicate that the effects of the gap junction blockers were not an artifact of the long time required for their action. These gap junction blockers are known to have some side effects[13,14], so the results must be interpreted with caution, but the common action of both drugs implicates gap junctions in either the integration of action potentials leading up to persistent firing or the generation of distal axonal action potentials during persistent firing. Hippocampal and neocortical interneurons are often connected by gap junctions[15], but in our paired recordings from EGFP-labeled interneurons, direct electrical coupling was usually not observed, including in the three pairs in which we observed persistent firing in the unstimulated neuron. For this reason, the relevant gap junctions may not be between the somata or dendrites. Instead, they could be located between axons[16] or between glial cells that may participate in persistent firing in some way[17–19]. Additional work will be required to elucidate the mechanisms of this form of persistent firing, including further investigation of the involvement of gap junctions.

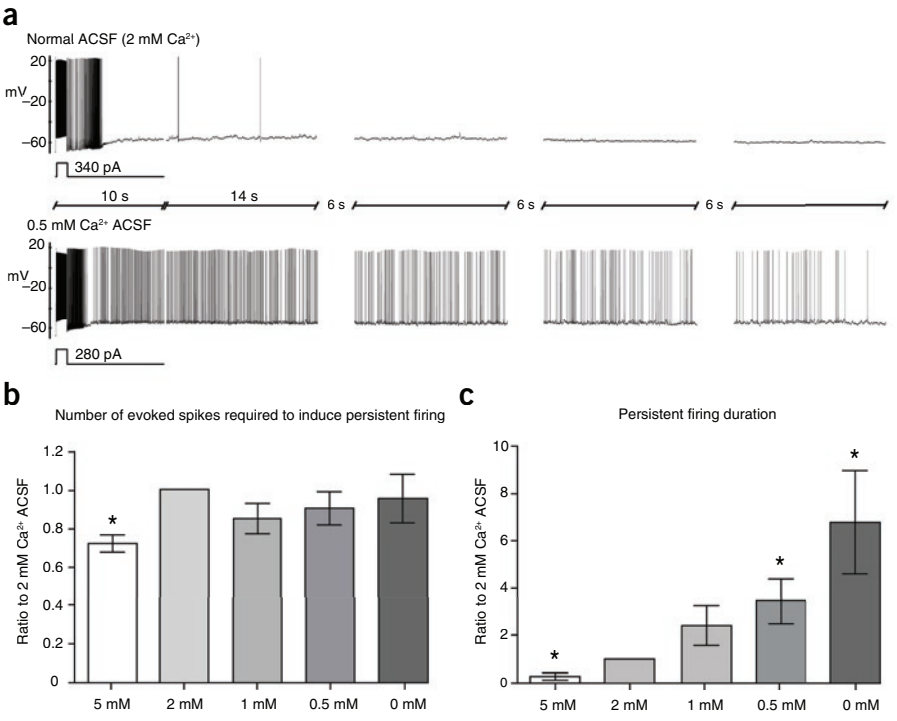

Figure 6 Calcium effects on persistent firing. (**a**) Recordings from an Htr5b-EGFP–positive hippocampal interneuron in normal (top; 2 mM) and low (bottom; 0.5 mM) Ca^{2+} artificial cerebrospinal fluid (ACSF). Note the firing lasts markedly longer in low Ca^{2+} than in normal ACSF. (**b**) Bar graph showing the number of evoked spikes required to induce persistent firing remains unchanged in low Ca^{2+} conditions (all data normalized to the 2 mM condition in the same cells; 1 mM, $n = 9$, 0.5 mM, $n = 11$; 0 mM, $n = 10$). Increasing the Ca^{2+} concentration to 5 mM slightly reduced the number of evoked spikes required to induce persistent firing ($n = 4$). (**c**) The duration of persistent firing was significantly increased in low Ca^{2+} (0.5 mM and 0 mM) and reduced in high Ca^{2+} (5 mM). All statistics are paired-sample comparisons relative to 2 mM Ca^{2+} in the same cell, $^*P < 0.05$. All summary data are mean ± s.e.m. All data are from Htr5b-EGFP–positive hippocampal interneurons near the stratum radiatum–SLM border.

DISCUSSION

Consolidating these results suggests the existence of a previously unknown operational mode for some mammalian neurons. A slow process integrates the occurrence of hundreds of stimulated action potentials over tens of seconds to minutes; this results in unstimulated action potential firing that begins abruptly and persists for tens of seconds to minutes. During persistent firing, action potentials are generated in the distal axon, presumably as a result of prolonged opening or closing of ion channels there. This form of firing can occur not just in the stimulated cell, but also in other cells. The mechanisms responsible for all aspects of this new operational mode are unknown and elucidating them will require extensive work.

Integrators that have long time constants and drive persistent action potential firing have been observed in many other systems, where they may arise from intrinsic cellular mechanisms, network mechanisms or both[20]. The mechanisms by which slow integration and persistent firing develop are poorly understood, but our findings expand the repertoire of possibilities to include mechanisms in or near the distal axon and mechanisms that can be shared by multiple neurons without a requirement for somatic or dendritic depolarization or synaptic interactions via ionotropic glutamate or GABA receptors.

In the mammalian CNS, previous reports of action potentials initiated in the distal axons have largely been in models of epilepsy, but a normal role has been proposed for bursting of thalamocortical neurons[9]. In sensory neurons of the dorsal root ganglion, firing of one cell can lead to firing of neighboring neurons without any synaptic interaction in the ganglion[2]. In invertebrate neurons, spikes can be initiated at multiple locations[6–8]; for example, in the crab stomatogastric ganglion, release of serotonin from a muscle can initiate action potentials in the axon terminals of motor neurons[8]. A similar mechanism could occur in our experiments, as previous work has demonstrated the existence of axonal neurotransmitter receptors that can influence presynaptic firing[6,7,21,22]; however, such an interaction would have to

be excitatory, despite the presumed inhibitory nature of these neurons. Other possibilities for the axo-axonal interactions include gap junctions[16] or the involvement of intermediary glial cells[17–19].

The ability of natural patterns of action potential firing to elicit persistent firing in interneurons suggests that it may occur *in vivo*. Spikelets have been reported in many previous studies, where they have been attributed to dendritic spikes, axonal spikes and spikes in cells coupled by gap junctions. Several studies have reported spikelets in hippocampal pyramidal neurons, both *in vitro* and *in vivo*[23,24], including recently in whole-cell recordings from awake, behaving rats[25]. Although we have not observed persistent firing in hippocampal pyramidal neurons, it is possible that a similar mechanism leads to axonally initiated spikes under other conditions. Our results in interneurons suggest that some previously described spikelets may reflect distal axonal action potentials that fail to invade the soma as full-sized action potentials.

Studying persistent axonal firing in interneurons using extracellular unit recording *in vivo* will require a means of identifying activity from these neurons. This may be difficult, not only because there are other interneurons in the same region that do not exhibit persistent firing, but also because interactions of persistent firing with ongoing synaptic activity (or neuromodulators) are likely to change its character under active conditions *in vivo* (**Fig. 2b**). A long-term goal will be to elucidate the mechanisms responsible for persistent firing *in vitro* and to determine how and when those mechanisms are activated *in vivo*.

If axons can integrate and share signals, what is the function of this interconnected network of axonal arborizations, capable of operating independently of the soma and dendrites? The fact that slow integration leads to persistent firing suggests three possible functions. First, persistent firing occurs at frequencies that match those of commonly observed oscillations (principally beta and gamma). These oscillations are thought to involve interneurons in the hippocampus and neocortex[26,27], so synchronization of populations of principal neurons by a network of interconnected inhibitory neurons could contribute to such oscillations. Persistent firing may therefore be involved in the generation of these oscillations, which have been implicated in cognitive processing and some psychiatric disorders[28]. Second, given the abundance of 'ectopic spikes' observed in models of epilepsy and the similarities of persistent firing to these events, it is possible that persistent firing is a protective mechanism engaged during seizures of similar bouts of hyperexcitability. Finally, the ability of axonally integrating interneurons to persistently fire without any ongoing stimulation provides a mechanism by which information could be stored over short periods of time, indicating a possible role in working memory, as has been suggested for other forms of persistent firing[29,30].

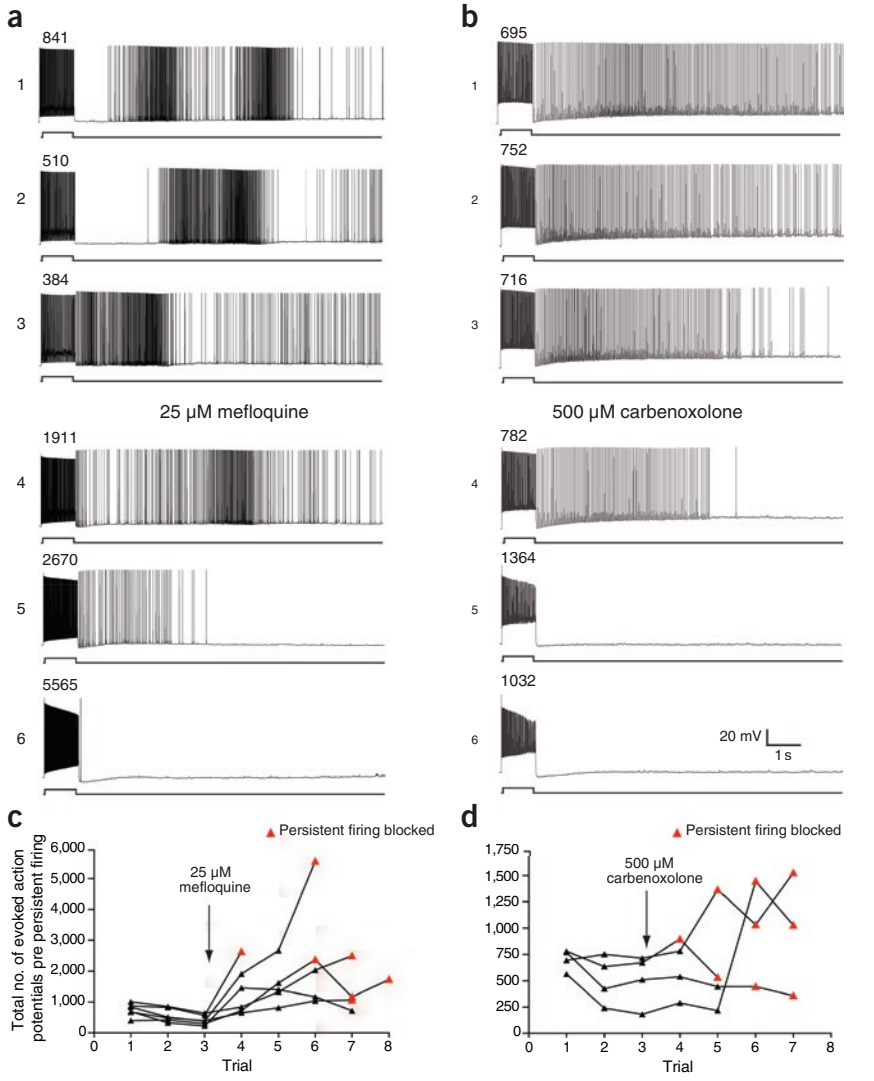

Figure 7 Gap junction blockers inhibit persistent firing. (**a**,**b**) Mefloquine (25 μM, **a**) and carbenoxolone (500 μM, **b**) were bath applied after three trials of persistent firing (sequential trial iteration indicated with number to the left of the trace) induction. Persistent firing was induced approximately once every 7 min (depending on how many spikes were required in each trial). The numbers above the evoked spikes indicate the total number of evoked action potentials for that trial. (**c**) The total number of evoked action potentials required to evoke persistent firing is plotted against the trial number (for 6 cells). Mefloquine (25 μM) was added to the bath after the third trial in each cell. In five out of the six cells persistent firing was not induced in the presence of mefloquine (represented by the red triangles indicating the maximum number of evoked spikes that was reached on that trial). (**d**) Carbenoxolone (500 μM) had a similar effect, preventing persistent firing in four out of four cells. All data are from Htr5b-EGFP–positive hippocampal interneurons near the stratum radiatum–SLM border.

METHODS

Methods and any associated references are available in the online version of the paper at http://www.nature.com/natureneuroscience/.

Note: Supplementary information is available on the Nature Neuroscience website.

ACKNOWLEDGMENTS

We thank T. Klausberger, S. Layton and M. Wilson for providing *in vivo* spiking data, and M. Benton, M. Nusbaum and members of the Spruston laboratory for helpful discussion and comments on the manuscript. We also thank E. Grodinsky for interneuron reconstructions. Grant support was provided by the US National Institutes of Health (NS-046064 to N.S. and W.L.K.) and the National Alliance for Research on Schizophrenia and Depression (N.S.). M.E.J.S. was supported by a Presidential Fellowship from Northwestern University.

AUTHOR CONTRIBUTIONS
All authors participated in the design of the experiments and the analysis and interpretation of the data. M.E.J.S. and T.K.B. performed the experiments. W.L.K. performed the simulations. N.S. and B.D.M. wrote the manuscript with input from the other authors.

COMPETING FINANCIAL INTERESTS
The authors declare no competing financial interests.

Published online at http://www.nature.com/natureneuroscience/.
Reprints and permissions information is available online at http://www.nature.com/reprintsandpermissions/.

1. Ramon y Cajal, S. *Histology of the Nervous System of Man and Vertebrates* (Oxford University Press, New York, 1995).
2. Devor, M. Unexplained peculiarities of the dorsal root ganglion. *Pain* **6**, S27–S35 (1999).
3. Grimes, W.N., Zhang, J., Graydon, C.W., Kachar, B. & Diamond, J.S. Retinal parallel processors: more than 100 independent microcircuits operate within a single interneuron. *Neuron* **65**, 873–885 (2010).
4. Shepherd, G.M., Chen, W.R., Willhite, D., Migliore, M. & Greer, C.A. The olfactory granule cell: from classical enigma to central role in olfactory processing. *Brain Res. Rev.* **55**, 373–382 (2007).
5. Stuart, G., Spruston, N., Sakmann, B. & Häusser, M. Action potential initiation and backpropagation in neurons of the mammalian CNS. *Trends Neurosci.* **20**, 125–131 (1997).
6. Bucher, D., Thirumalai, V. & Marder, E. Axonal dopamine receptors activate peripheral spike initiation in a stomatogastric motor neuron. *J. Neurosci.* **23**, 6866–6875 (2003).
7. Goaillard, J.-M., Schulz, D.J., Kilman, V.L. & Marder, E. Octopamine modulates the axons of modulatory projection neurons. *J. Neurosci.* **24**, 7063–7073 (2004).
8. Meyrand, P., Weimann, J.M. & Marder, E. Multiple axonal spike initiation zones in a motor neuron: serotonin activation. *J. Neurosci.* **12**, 2803–2812 (1992).
9. Pinault, D. Backpropagation of action potentials generated at ectopic axonal loci: hypothesis that axon terminals integrate local environmental signals. *Brain Res. Brain Res. Rev.* **21**, 42–92 (1995).
10. Heintz, N. Gene expression nervous system atlas (GENSAT). *Nat. Neurosci.* **7**, 483 (2004).
11. Klausberger, T. & Somogyi, P. Neuronal diversity and temporal dynamics: the unity of hippocampal circuit operations. *Science* **321**, 53–57 (2008).
12. Klausberger, T. *et al.* Complementary roles of cholecystokinin- and parvalbumin-expressing GABAergic neurons in hippocampal network oscillations. *J. Neurosci.* **25**, 9782–9793 (2005).
13. Cruikshank, S.J. *et al.* Potent block of Cx36 and Cx50 gap junction channels by mefloquine. *Proc. Natl. Acad. Sci. USA* **101**, 12364–12369 (2004).
14. Tovar, K.R., Maher, B.J. & Westbrook, G.L. Direct actions of carbenoxolone on synaptic transmission and neuronal membrane properties. *J. Neurophysiol.* **102**, 974–978 (2009).
15. Hestrin, S. & Galarreta, M. Electrical synapses define networks of neocortical GABAergic neurons. *Trends Neurosci.* **28**, 304–309 (2005).
16. Schmitz, D. *et al.* Axo-axonal coupling: a novel mechanism for ultrafast neuronal communication. *Neuron* **31**, 831–840 (2001).
17. Bullock, T.H. *et al.* Neuroscience. The neuron doctrine, redux. *Science* **310**, 791–793 (2005).
18. Fields, R.D. Oligodendrocytes changing the rules: action potentials in glia and oligodendrocytes controlling action potentials. *Neuroscientist* **14**, 540–543 (2008).
19. Halassa, M.M. & Haydon, P.G. Integrated brain circuits: astrocytic networks modulate neuronal activity and behavior. *Annu. Rev. Physiol.* **72**, 335–355 (2010).
20. Major, G. & Tank, D. Persistent neural activity: prevalence and mechanisms. *Curr. Opin. Neurobiol.* **14**, 675–684 (2004).
21. Kullmann, D.M. Presynaptic kainate receptors in the hippocampus: slowly emerging from obscurity. *Neuron* **32**, 561–564 (2001).
22. Semyanov, A. & Kullmann, D.M. Kainate receptor–dependent axonal depolarization and action potential initiation in interneurons. *Nat. Neurosci.* **4**, 718–723 (2001).
23. Keros, S. & Hablitz, J.J. Ectopic action potential generation in cortical interneurons during synchronized GABA responses. *Neuroscience* **131**, 833–842 (2005).
24. MacVicar, B.A. & Dudek, F.E. Electrotonic coupling between pyramidal cells: a direct demonstration in rat hippocampal slices. *Science* **213**, 782–785 (1981).
25. Epsztein, J., Lee, A.K., Chorev, E. & Brecht, M. Impact of spikelets on hippocampal CA1 pyramidal cell activity during spatial exploration. *Science* **327**, 474–477 (2010).
26. Bartos, M. *et al.* Fast synaptic inhibition promotes synchronized gamma oscillations in hippocampal interneuron networks. *Proc. Natl. Acad. Sci. USA* **99**, 13222–13227 (2002).
27. McBain, C.J. & Fisahn, A. Interneurons unbound. *Nat. Rev. Neurosci.* **2**, 11–23 (2001).
28. Lisman, J.E. *et al.* Circuit-based framework for understanding neurotransmitter and risk gene interactions in schizophrenia. *Trends Neurosci.* **31**, 234–242 (2008).
29. Durstewitz, D., Seamans, J.K. & Sejnowski, T.J. Neurocomputational models of working memory. *Nat. Neurosci.* **3 Suppl**, 1184–1191 (2000).
30. Egorov, A.V., Hamam, B.N., Fransén, E., Hasselmo, M.E. & Alonso, A.A. Graded persistent activity in entorhinal cortex neurons. *Nature* **420**, 173–178 (2002).

ONLINE METHODS

All experiments were approved by the Northwestern University Animal Care and Use Committee.

Hippocampal slice preparation. Parasagittal slices (~300 μm, hippocampus and neocortex) were prepared from postnatal day 14–30 (Htr5b-EGFP BAC transgenic) mice anesthetized with halothane or isoflurane. Alternatively, where indicated, Drd2-EGFP BAC transgenic mice, C57BL/6 mice or Wistar rats were used. Briefly, the animals were decapitated and the brains were rapidly removed and placed under ice-cold, sucrose-rich slicing solution containing 85 mM NaCl, 2.5 mM KCl, 1.25 mM NaH_2PO_4, 25 mM $NaHCO_3$, 25 mM glucose, 75 mM sucrose, 0.5 mM $CaCl_2$ and 4 mM $MgCl_2$ bubbled with 95%/5% O_2/CO_2. After slices were made they were transferred to a warmed (30 °C) incubation chamber with bubbled ACSF consisting of 125 mM NaCl, 2.5 mM KCl, 25 mM $NaHCO_3$, 1.25 mM NaH_2PO_4, 1 mM $MgCl_2$, 2 mM $CaCl_2$ and 25 mM dextrose for 20 min, after which the slices were removed to bubbled, 20–22 °C ACSF where they were maintained until placed in the recording chamber.

Hippocampal slice electrophysiology. During recording, slices were bathed in bubbled ACSF and maintained at a constant temperature ranging from 30–37 °C. We saw no persistent firing when recordings performed at 20–22 °C (n = 20). Somatic whole-cell current-clamp recordings were made using patch-clamp electrodes pulled from borosilicate glass and filled with intracellular solution containing 135 mM potassium gluconate, 7.5 mM KCl, 10 mM sodium phosphocreatine, 10 mM HEPES, 2 mM MgATP, 0.3 mM NaGTP and 0.5% mM biocytin. Recordings were made using one or two bridge amplifiers (BVC-700, Dagan). Electrode resistance in the bath was 3–7 MΩ and series resistance was 15–35 MΩ; the resultant errors were minimized using bridge balance and capacitance compensation. Electrophysiological traces were digitized by an ITC-16 board (Instrutech) under control of custom macros programmed in IGOR Pro software (WaveMetrics). During the stimulation protocol, cells were maintained at a membrane potential between –65 and –70 mV with holding current when needed (from 0 to ±100 pA, negative in >95% of recordings). We delivered 1-s current pulses at the beginning of ten-second sweeps, in most cases starting at 40 or 50 pA and incrementing by 20 pA up to a maximum of 800 pA. If the current stimulus initiated persistent firing (>8 Hz firing for at least 1 s), no subsequent stimulation was delivered and the cell was allowed to fire for up to 4 min before the protocol was run again after a recovery interval of several minutes, starting again with the initial current injection step followed by subsequent 20-pA incremental steps. In some cases, persistent firing was induced using successive stimulation with a larger current step (**Fig. 1a**). When persistent firing was induced multiple times in the same cell, a period of 2–3 min was typically included between the cessation of persistent firing and the next round of stimulation.

***In vivo* firing patterns.** Data for low frequency stimulus pattern (mean firing rate of 5.8 Hz) was provided by T. Klausberger (unpublished data), cell T82e[12] recorded from an interneuron *in vivo* near the stratum radiatum–SLM border of CA1 in an anaesthetized rat. This firing pattern was recapitulated in the slice using brief current injections (1 ms, 800 pA; **Fig. 2a**).

Data for the high-frequency stimulus pattern (mean firing rate of 33.4 Hz) was provided by S. Layton and M. Wilson (unpublished data), recorded from an interneuron in the hippocampus of an awake running rat. This firing pattern was recapitulated in the slice using brief current injections (1 ms, 1,000 pA). Each 10-s sweep contained up to 8 s of stimulation, but the duration of the firing pattern could be adjusted in those cells that generated persistent firing on the first sweep and required less than 8 s of stimulation. **Figure 4b** is an example of persistent firing evoked by just 4 s of this stimulus pattern.

For within-cell comparisons in **Figure 4**, we only included cells in which all three stimulation protocols were successful at inducing persistent firing. To compare differences in these cases, we used a one-way repeated-measures ANOVA with Tukey's *post hoc* comparisons. In some cases, it was not possible to evoke persistent firing with all three protocols; we therefore grouped all cells in which two or more protocols were compared using a one-way ANOVA with Tukey's *post hoc* comparisons.

Pharmacology. Where indicated, drugs were added to ACSF at noted concentrations and applied via the bath to test their effects on persistent firing. For antidromic stimulation, 4 μM SR95531 (Sigma-Aldrich), 1 μM CGP52432 (Tocris), 25 μM CNQX (Tocris) and 50 μM D-AP5 (Tocris) were added to the ACSF for pharmacological blockade of $GABA_A$, $GABA_B$, AMPA, kainate and NMDA receptors, respectively. To examine calcium effects, the Ca^{2+} ($CaCl_2$) concentration in ACSF was adjusted and replaced with equimolar Mg^{2+} ($MgCl_2$).

Data analysis and statistics. Analyses of electrophysiology data were performed using custom programs in IGOR Pro software and statistical analyses were performed using Prism 4 software (GraphPad). Pooled data from multiple cells were tested for significant differences using either paired or unpaired Student's t tests, or a one-way ANOVA with Tukey's *post hoc* comparisons. For all statistical tests, significance was $P < 0.05$. All measurements are presented as mean ± s.e.m. unless otherwise indicated. To determine the statistical significance of persistent firing in unstimulated neurons during paired recordings (n = 3 of 19), we compared this rate to the occurrence of spontaneous persistent firing (that is, before stimulation) in unpaired recordings (n = 0/274) using Fisher's and Barnard's exact tests, giving resulting two-sided P values of 0.00023 and 0.00012, respectively. Thus, it is extremely unlikely that the persistent firing observed in unstimulated neurons during paired recordings is not caused by stimulation of the other cell.

Computational models. All numerical simulations were performed with the computational software NEURON[31] using the variable time step (CVODE) method.

For the stylized model, the morphology consisted of a spherical soma (14 μm in diameter) connected to a primary axon with a length of 1,060 μm (0.4 μm in diameter). Starting 40 μm away from the soma, five 200-μm-long, 0.5-μm diameter side branches bifurcated from the main axon, separated from one another by a distance of 5 μm. In all compartments, the specific membrane capacitance was 1 μF cm^{-2}, axial resistivity was 100 Ωcm, and membrane resistivity was 10,000 Ωcm^2. Following experimental results from fast-spiking cortical interneurons[32], Na, Kv3.1-Kv3.2 and Kv1.3 channels were inserted into the neuronal membrane with varying densities, with the modification that both activation and inactivation of the Na channel were sped up by a factor of two so that the shape of the results in the computational phase plot ($dV\,dt^{-1}$ versus V) better matched the experimental results. In all simulations, the values of $dV\,dt^{-1}$ were obtained by dividing somatic membrane current density by specific membrane capacitance. The Na channel densities were 10 mS cm^{-2} in the soma and 80 mS cm^{-2} in the axon. The Kv3 channel densities were 80 mS cm^{-2} in the soma and 100 mS cm^{-2} in the axon. The Kv1.3 channel densities were 2 mS cm^{-2} in the soma, 1 mS cm^{-2} in the proximal 60 μm of the axon and 0 mS cm^{-2} in the remainder. The Na and K channel reversal potentials were assumed to be +55 mV and –85 mV, respectively. The stylized model neuron was stimulated with constant current injections of –55 pA in the soma and 15 pA in the axon located 960 μm from the soma (**Fig. 2**). The parameters of the model were tuned so that antidromic axonal action potentials were generated and produced a repeating pattern consisting of a full somatic action potential, an antidromic action potential that failed at the soma, and three antidromic action potentials that failed at an axonal branch point. Other parameter values could produce either a single repeating behavior or a pattern with a different combination of the three behaviors.

In the morphological model, the stylized interneuron was replaced with the morphology of a reconstructed interneuron with a cell body near the stratum radiatum–SLM border of CA1. This interneuron was visualized using the DAB reaction using standard procedures and reconstructed using a Zeiss microscope (63× oil immersion objective) fitted with semi-automated Neurolucida hardware and software (version 6, MicroBrightField). Although the axon was extensively stained, portions of the axon were only weakly visible; as a result, judgment and consistency with the strongly visible parts of the axonal arborization were used to obtain complete connectivity. To form an initial segment, the diameter of the axon at the soma was assumed to be 1 μm and then to taper to 0.5 μm at a distance 17.5 μm from the soma. The 0.5-μm diameter was continued in the primary axon to a distance of 35 μm from, at which point it tapered linearly to 0.34 μm at a distance of 67 μm from the soma. A diameter of 0.34 μm was used in all other branches of the axonal arborization. In all compartments, the membrane capacitance was 0.9 μF cm^{-2}, the axial resistivity was 100 Ωcm, and the membrane resistivity was 5,000 Ωcm^2. Na and Kv3 channels as described for the stylized model were inserted in the cell membrane (but no Kv1.3 channels were used). In this model, the Na channel density was 50 mS cm^{-2} in the soma and 10 mS cm^{-2} in the dendrites. In the axon, for the first 20 μm, the density of Na

doi:10.1038/nn.2728

channels was 600 mS cm^{-2} and in the next 20 µm it was 250 mS cm^{-2}. From 40 µm to 60 µm the density decreased linearly to 100 mS cm^{-2}, a value that was used in all other branches of the axonal arborization. The densities used for the Kv3 channel were 100 mS cm^{-2} in the soma and dendrites, 1,000 mS cm^{-2} in the first 20 µm of the axon, 500 mS cm^{-2} in the next 20 µm; from 40 to 60 µm the density in the axon decreased linearly to 200 mS cm^{-2}, a value that was used in all other branches of the axonal arborization. The Na and K channel reversal potentials were again assumed to be +55 mV and –85 mV, respectively. The morphological model neuron was stimulated with constant current injections of –200 pA in the soma and 25 pA in the axon, 325 µm away from the soma. As for the stylized model, the parameters of the model were tuned so that antidromic axonal action potentials were generated and produced a repeating pattern consisting of a full somatic action potential, an antidromic action potential that failed at the soma, and an antidromic action potential that failed at an axonal branch point. Other parameter values could produce either a single repeating behavior or patterns with different combinations of the three behaviors.

31. Hines, M.L. & Carnevale, N.T. The NEURON simulation environment. *Neural Comput.* **9**, 1179–1209 (1997).
32. Erisir, A., Lau, D., Rudy, B. & Leonard, C.S. Function of specific K(+) channels in sustained high-frequency firing of fast-spiking neocortical interneurons. *J. Neurophysiol.* **82**, 2476–2489 (1999).